

Characterization of welding defects by fractal analysis of ultrasonic signals

A. P. Vieira, E. P. de Moura, L. L. Gonçalves

Departamento de Engenharia Metalúrgica e de Materiais, Universidade Federal do Ceará, Fortaleza, CE, Brazil

J. M. A. Rebello

Departamento de Engenharia Metalúrgica e de Materiais, Universidade Federal do Rio de Janeiro, RJ, Brazil

Abstract

In this work we apply tools developed for the study of fractal properties of time series to the problem of classifying defects in welding joints probed by ultrasonic techniques. We employ the fractal tools in a preprocessing step, producing curves with a considerably smaller number of points than in the original signals. These curves are then used in the classification step, which is realized by applying an extension of the Karhunen-Loève linear transformation. We show that our approach leads to small error rates, comparable with those obtained by using more time-consuming methods based on non-linear classifiers.

1 Introduction

Ultrasonic tests can serve as a useful tool for evaluating the integrity of metallic structures, and specially of weld joints. By inspecting the scattering pattern of ultrasonic waves propagating in the material, it is possible to identify the presence of defects, and to estimate their dimensions. However, it is often desirable to have precise information about the nature of the defects, and a number of studies have tried to propose useful approaches to perform such classification [1,2,3,4], mostly based on direct analysis of the patterns with neural networks.

In the present paper, we describe a distinct approach, based on tools developed for analyzing fractal properties of time series [5,6,7,8]. Such kind of approach has been successfully applied to ultrasonic signals (interpreted as a particular kind of time series) by a number of authors [9,10,11], both in defect and in

microstructure classification, by calculating the exponents of the power laws characterizing various fractal features of the series, and hoping to associate different sets of exponents with different classes. However, this can only be expected to work when the typical series corresponding to different classes are highly dissimilar, due to the fact that the size of each series is usually small, and estimates of the various exponents are subject to significant fluctuations. Thus, in general, an expanded set of features must be used to obtain an efficient classification algorithm. Here we employ tools from the statistical pattern-classification literature to extract relevant features from the set of fractal analyses applied to ultrasonic signals obtained from weld joints having three different kinds of defects.

We used 240 ultrasonic signals obtained by the TOFD technique [12], with 60 signals corresponding to each kind of defect (lack of fusion, lack of penetration, and porosity) and other 60 signals from regions with no defects. (For a description of the materials used, as well as techniques for producing and capturing the signals, see Ref. [3].) All signals had a length of 512 points, with 8-bit resolution. Typical signals are shown in Fig. 1. After normalizing all signals so that the maximum and minimum values correspond to 1 and -1 , we calculated the corresponding curves from four different techniques of fractal analysis, which we describe in Sec. 2. Then, as described in Sec. 3, we employed a variation of the Karhunen-Loève (KT) linear transformation [13,14] to extract relevant features from the curves. As we discuss in the final section, the combined approach of fractal analysis and KT transformation yields a quite good classification tool for the defects studied.

2 Fractal analysis

All techniques of fractal analysis employed here start by dividing the signal into intervals containing τ points. Each technique then involves the calculation of the average of some quantity $Q(\tau)$ over all intervals, for different values of τ . In a signal with genuine fractal features, $Q(\tau)$ should scale as a power of τ ,

$$Q(\tau) \sim \tau^\eta, \tag{1}$$

at least in an intermediate interval of values of τ , corresponding to $1 \ll \tau \ll L$, L being the signal length.

Fractals of different nature should give rise to different exponents η , providing a signature of the fractal. In our case, due to the finite amount of points, and to the very nature of the signals, a pure power-law behavior is hard to observe. Instead, as shown in Fig. 2, the curves usually exhibit features such

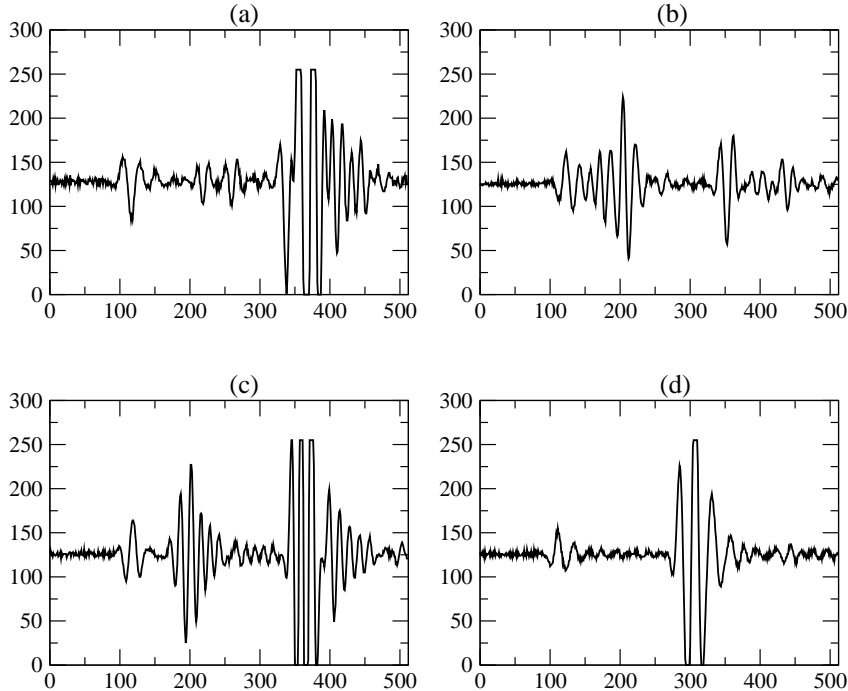


Figure 1. Typical examples of signals obtained from samples with (a) lack-of-fusion defects, (b) lack-of-penetration defects, (c) porosities, and (d) no defects. The horizontal axes correspond to the time direction, in units of the inverse sample rate of the equipment.

as a crossover between different power-law behaviors, or saturation points, which can also serve as signatures of the different kinds of defects. However, identifying the relevant features in advance is a complex task. Fortunately, the pattern-classification literature offers useful tools for feature extraction from data, and we describe one of those in Sec. 3 and Appendix A.

2.1 Hurst (R/S) analysis

The rescaled-range (R/S) analysis was introduced by Hurst [5] as a tool for evaluating the persistency or antipersistency of a time series. The method works by dividing the series into intervals of a given size, and calculating the average ratio of the range (the difference between the maximum and minimum values of the series) to the standard deviation inside each interval. The size of each interval is then varied.

Mathematically, the R/S analysis is defined in the following way. Given an interval of size τ , whose left end is located at point i_0 , we calculate $\langle z \rangle_\tau$, the

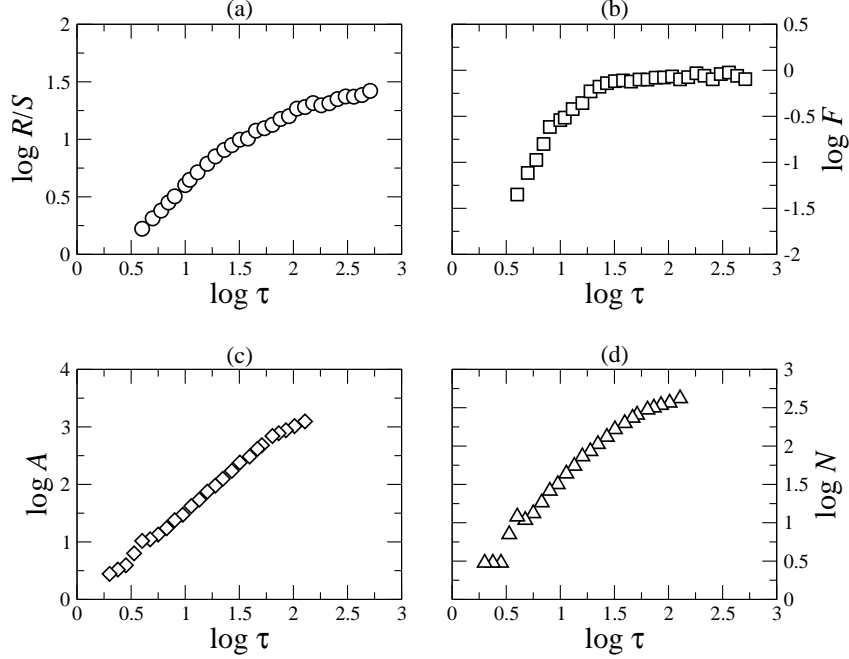


Figure 2. Curves for a lack-of-fusion signal, obtained from (a) Hurst analysis, (b) detrended-fluctuation analysis, (c) minimal-cover analysis, and (d) box-counting analysis.

average of the series z_i inside the interval,

$$\langle z \rangle_\tau = \frac{1}{\tau} \sum_{i=i_0}^{i_0+\tau-1} z_i. \quad (2)$$

We then define an accumulated deviation from the mean as

$$Z_i = \sum_{k=i_0}^i (z_k - \langle z \rangle_\tau), \quad (3)$$

from which we extract a range,

$$R(\tau) = \max_{i_0 \leq i \leq i_0+\tau-1} Z_i - \min_{i_0 \leq i \leq i_0+\tau-1} Z_i, \quad (4)$$

and the corresponding standard deviation,

$$S(\tau) = \sqrt{\frac{1}{\tau} \sum_{i=i_0}^{i_0+\tau-1} Z_i^2}. \quad (5)$$

Finally, we obtain the rescaled range $R(\tau)/S(\tau)$, and take its average over all intervals.

For a curve with true fractal features, the rescaled range should satisfy the scaling form

$$\frac{R(\tau)}{S(\tau)} \sim \tau^H, \quad (6)$$

where H is the Hurst exponent.

A typical curve obtained from the R/S analysis of the signals is shown in Fig. 2(a).

2.2 Detrended-fluctuation analysis

The detrended-fluctuation analysis (DFA) [6] aims to improve the evaluation of correlations in a time series by eliminating trends in the data.

The method consists initially in obtaining a new integrated series \tilde{z}_i ,

$$\tilde{z}_i = \sum_{k=1}^i (z_k - \langle z \rangle), \quad (7)$$

the average $\langle z \rangle$ being taken over all points,

$$\langle z \rangle = \frac{1}{L} \sum_{i=1}^L z_i. \quad (8)$$

After dividing the series into intervals, the points inside a given interval are fitted by a polynomial curve of degree n . In our case, we have considered $n = 1$ or $n = 2$, corresponding to first- and second-order fits. Then, a detrended variation function $\Delta_{i,n}$ is obtained by subtracting from the integrated data the local trend as given by the fit. Explicitly, we define

$$\Delta_{i,n} = \tilde{z}_i - h_{i,n}, \quad (9)$$

where $h_{i,n}$ is the value associated with point i according to the fit of degree n . Finally, we calculate the root-mean-square fluctuation $F_n(\tau)$ inside an interval as

$$F_n(\tau) = \sqrt{\frac{1}{\tau} \sum_i \Delta_{i,n}^2}, \quad (10)$$

and average over all intervals. For a true fractal curve, $F(\tau)$ should behave as

$$F(\tau) \sim \tau^\alpha, \quad (11)$$

where α is the scaling exponent.

A typical curve obtained from the detrended-fluctuation analysis of the signals is shown in Fig. 2(b).

2.3 Minimal-cover analysis

This recently introduced method [7] relies on the calculation of the minimal area necessary to cover a given plane curve at a specified scale.

After dividing the series, we can associate with each interval, labeled by a variable k , a rectangle of height H_k , defined as the difference between the maximum and minimum values of the series z_i inside the k th interval,

$$H_k = \max_{i_0 \leq i \leq i_0 + \tau - 1} z_i - \min_{i_0 \leq i \leq i_0 + \tau - 1} z_i, \quad (12)$$

in which $i_0 = 1 + (k - 1)\tau$ labels the left end of the interval. The minimal area is then given by

$$A(\tau) = \sum_k H_k \tau, \quad (13)$$

the summation running over all cells.

Ideally, in the scaling region, $A(\tau)$ should behave as

$$A(\tau) \sim \tau^{2-D_\mu}, \quad (14)$$

where D_μ is the minimal cover dimension, which is equal to 1 when the signal presents no fractality.

A typical curve obtained from the minimal-cover analysis of a signal is shown in Fig. 2(c).

2.4 Box-counting analysis

This is a well-known method of estimating the fractal dimension of a point set [8], and it works by counting the minimum number $N(\tau)$ of boxes of side τ needed to cover all points in the set. For a real fractal, $N(\tau)$ should follow a power law whose exponent is the box-counting dimension D_B ,

$$N(\tau) \sim \tau^{-D_B}. \quad (15)$$

A typical box-counting curve for a signal is shown in Fig. 2(d).

3 Results of the classification approach

In order to classify the signals, we used a supervised variation of the Karhunen-Loève (KL) transformation [13,14], briefly described in Appendix A. For each signal, we collected the corresponding curves from various fractal analyses, forming a single vector with M components. The most successful combination involves curves from Hurst, linear detrended-fluctuation, minimal-cover, and box-counting analyses, corresponding to $M = 108$ (with 27 components of the vector taken from each curve). A plot obtained by projecting the first two components of the KL-transformed vectors is shown in Fig. 3, for the full set of vectors. (Note that, with 4 different classes for the vectors, the transformed space is three-dimensional.) It is evident from the figure that the transformation yields a good clustering of the vectors around the different class means. This clustering is a general feature of the KL transformation. However, to assess the utility of the classification approach, it is essential to evaluate the generalization error.

We proceeded by first randomly dividing the vectors into a training set (with 80% of the signals) and a test set (with the remaining signals). The KL transformation was first applied to the training vectors, and the class means were determined. Transformed vectors in both sets were then classified by applying the nearest-class-mean rule, i.e., a vector \mathbf{x} was assigned to the class whose average vector, as determined by the training set, lies closer to \mathbf{x} . (It is also possible to explore other approaches for discrimination, such as Bayesian rules, but that would require an estimation of the class-conditional probabilities, which we do not have at hand.) Finally, we took averages over 500 different choices of training and test sets.

The average confusion matrices of the training and test sets are shown in Tables 1 and 2. Notice that the mean error rate is negligible for the training vectors, and corresponds to around 15% for the test vectors. These error rates

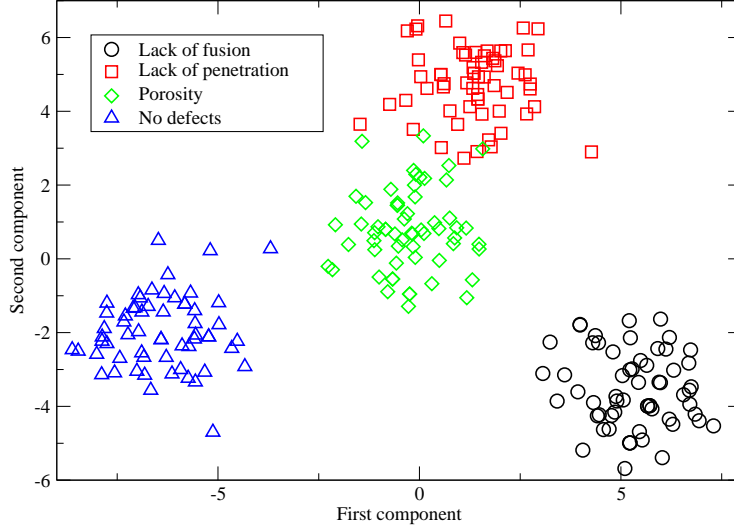


Figure 3. Projection, along the first two components, of the vectors obtained by applying the Karhunen-Loève transformation to the full data set obtained from four different fractal analyses.

Table 1

Average confusion matrix for the training vectors, derived from the fractal analyses. The possible classes are lack of fusion (LF), lack of penetration (LP), porosity (PO) and no defects (ND). The figures in parenthesis indicate the standard deviations, calculated over 500 sets. The value in row i , column j indicates the percentage of vectors belonging to class i which were associated with class j .

	LF	LP	PO	ND
LF	100	0	0	0
LP	0	99.87 (0.50)	0.13 (0.50)	0
PO	0	0.01 (0.10)	99.99 (0.10)	0
ND	0	0	0.01 (0.08)	99.99 (0.08)

are comparable to those obtained by analyzing the same signals directly using non-linear classifiers based on neural networks [4]; the use of linear classifiers, on the other hand, leads to considerably higher error rates [3]. Notice that in our study the number of variables (108) employed in the classification step represents only around 1/5 of the number used in the neural-network studies (which made use of all 512 points of each signal). Besides rendering the calculations faster, for an equivalent error rate, the smaller number of variables also leads to smaller fluctuations in the curves.

For completeness, we also applied the KT transformation to both the correlograms and the Fourier spectra of each signal, obtaining average error rates no smaller than 36% and 48%, respectively (see Table 3).

Table 2

The same as in Table 1, for the testing vectors.

	LF	LP	PO	ND
LF	91.07 (8.20)	1.69 (3.64)	6.88 (7.37)	0.35 (1.69)
LP	2.61 (8.20)	83.96 (10.04)	12.14 (9.27)	1.28 (3.21)
PO	6.43 (7.27)	13.99 (10.5)	72.66 (12.87)	6.92 (7.55)
ND	1.01 (3.25)	2.55 (4.43)	6.92 (7.16)	89.51 (8.93)

Table 3

Average percentage rates of correct classification of the test vectors, derived from applying the KL transformation to the correlograms or the Fourier spectra associated with the signals. The figures in parenthesis indicate standard deviations calculated over 100 sets.

	LF	LP	PO	ND
Correlograms	60.19 (17.75)	64.18 (14.96)	51.60 (16.87)	57.43 (16.16)
Fourier spectra	51.42 (17.49)	47.35 (17.03)	46.76 (16.64)	48.08 (15.76)

4 Conclusions

In this paper we applied techniques developed for the study of fractal properties of time series as a preprocessing tool for the classification of defects probed by ultrasonic signals. The signals were obtained in welding joints containing three different classes of defects, and we also considered signals with no defects. For the classification step, we employed an extension of the Karhunen-Loève transformation, which, supplemented by the nearest-class-mean rule, yielded low error rates (between 0 and 15%) both in the training and the test stages. These error rates are comparable with those obtained from more time-consuming approaches based on direct analysis of the signals. In our view, this is evidence that fractal techniques are a promising tool for the classification of defects probed by ultrasonic inspection.

We believe that the performance of the classification approach based on fractal techniques can be further improved by resorting to non-linear classifiers, especially in combination with reclassification and hierarchical procedures. These extensions we leave for future investigations.

Acknowledgements

We acknowledge financial support from the Brazilian agencies FUNCAP, CNPq, CAPES and FINEP (CT-Petro). A. P. Vieira has benefitted from helpful con-

versations with N. Caticha.

A Karhunen-Loève transformation

The Karhunen-Loève (KL) transformation, as the principal component analysis, is a tool for feature selection and extraction. It produces a set of mutually uncorrelated components, and dimensionality reduction can be achieved by selecting those components with the largest variances. The version of the transformation employed here [Kittler and Young, 1973 (Webb)] relies on compression of the discriminatory information contained in the class means.

Let \mathbf{x}_i be the (column) vector corresponding to the i th signal. The KL transformation consists of first projecting the training vectors along the eigenvectors of the within-class covariance matrix \mathbf{S}_W , defined by

$$\mathbf{S}_W = \frac{1}{N} \sum_{k=1}^{N_C} \sum_{i=1}^{N_k} y_{ik} (\mathbf{x}_i - \mathbf{m}_k)(\mathbf{x}_i - \mathbf{m}_k)^T, \quad (\text{A.1})$$

where N_C is the number of different classes, N_k is the number of vectors in class k , \mathbf{m}_k is the average vector of class k , and T denotes the transpose of a matrix (in this case, yielding a row vector). The element y_{ik} is equal to one if \mathbf{x}_i belongs to class k , and zero otherwise. We also rescale the resulting vectors by a diagonal matrix built from the eigenvalues λ_j of \mathbf{S}_W . In matrix notation, this operation can be written as

$$\mathbf{X}' = \Lambda^{-\frac{1}{2}} \mathbf{U}^T \mathbf{X}, \quad (\text{A.2})$$

in which \mathbf{X} is the matrix whose columns are the training vectors \mathbf{x}_i , $\Lambda = \text{diag}(\lambda_1, \lambda_2, \dots)$, and \mathbf{U} is the matrix whose columns are the eigenvectors of \mathbf{S}_W . This choice of coordinates makes sure that the transformed within-class covariance matrix corresponds to the unit matrix. Finally, in order to compress the class information, we project the resulting vectors onto the eigenvectors of the between-class covariance matrix \mathbf{S}_B ,

$$\mathbf{S}_B = \sum_{k=1}^{N_C} \frac{N_k}{N} (\mathbf{m}_k - \mathbf{m})(\mathbf{m}_k - \mathbf{m})^T, \quad (\text{A.3})$$

where \mathbf{m} is the overall average vector. The full transformation can be written as

$$\mathbf{X}'' = \mathbf{V}^T \Lambda^{-\frac{1}{2}} \mathbf{U}^T \mathbf{X}, \quad (\text{A.4})$$

\mathbf{V} being the matrix whose columns are the eigenvectors of \mathbf{S}_B (calculated from \mathbf{X}').

With N_C possible classes, the fully-transformed vectors have at most $N_C - 1$ relevant components. We then associate a vector \mathbf{x}_i with the class whose average vector lies closer to \mathbf{x}_i within the transformed $(N_C - 1)$ -dimensional space. This association rule would be optimal if the vectors in different classes followed normal distributions.

References

- [1] A. Masnata and M. Sunseri. *NDT&E International*, 29:87–93, 1996.
- [2] F. W. Margrave, K. Rigas, D. A. Bradley, and P. Barrowcliffe. *Measurement*, 25:143–154, 1999.
- [3] E. P. de Moura, M. H. S. Siqueira, R. R. da Silva, J. M. A. Rebello, and L. P. Calôba. *Insight*, 47:777–782, 2005.
- [4] E. P. de Moura, M. H. S. Siqueira, R. R. da Silva, and J. M. A. Rebello. *Insight*, 47:783–787, 2005.
- [5] H. E. Hurst. *Trans. Am. Soc. Civ. Eng.*, 116:770–799, 1951.
- [6] C. K. Peng, V. Buldyrev, S. Havlin, M. Simmons, H. E. Stanley, and A. L. Goldberger. *Phys. Rev. E*, 49:1685–1689, 1994.
- [7] P. M. Dubovikov, N. V. Starchenko, and M. S. Dubovikov. *Physica A*, 339:591–608, 2004.
- [8] P. S. Addison. *Fractals and Chaos*. IOP, London, 1997.
- [9] P. Barat. *Chaos, Solitons & Fractals*, 9:1827–1834, 2004.
- [10] J. M. O. Matos, E. P. de Moura, S. E. Krüger, and J. M. A. Rebello. *Chaos, Solitons & Fractals*, 19:55–60, 2004.
- [11] F. E. Silva, L. L. Gonçalves, D. B. B. Ferreira, and J. M. A. Rebello. *Chaos, Solitons & Fractals*, 26:481–494, 2005.
- [12] M. G. Silk. In R. S. Sharpe, editor, *Research Techniques in NDT*, volume III, page 51. Academic Press, London, 1976.
- [13] J. Kittler and P. C. Young. *Pattern Recognition*, 5:335–352, 1973.
- [14] A. R. Webb. *Statistical Pattern Recognition, 2nd ed.* John Wiley & Sons, West Sussex, 2002.